What's New!

August 30, 2016	Presentation data of Plenary talks and Tutorial talks are available to download. (participants only)
July 7, 2016	Best Paper Award and IEEE Photonics Society Japan Young Scientist Award Papers have been announced. Congratulations!!
July 6, 2016	Accepted Post Deadline Papers (PDP) are available to download.

Important Dates

Paper Submission starts .... December 20, 2015

Paper Submission Due Date .... ~~February 29, 2016~~ March 14, 2016

Acceptance Notification .... End of April, 2016

Post Deadline Paper(PDP) Submission Due Date .... June 20, 2016

PDP Acceptance Notification .... July 4, 2016

Sponsored by

Co-sponsored by :

Communications Society

Electronics Society

The Institute of Electronics, Information and Communication Engineers

Technically co-sponsored by :

IEEE ComSoc IEEE Communications Society

IEEE Photonics Society

OSA The Optical Society

in cooperation with :

CIAJ

Information Processing Society of Japan

IEEJ

ITE

The Japan Society of Applied Physics

OSJ

OITDA 一般財団法人 光産業技術振興協会

PHOTONIC INTERNET FORUM

SICE

IEEE Communications Society Japan Chapter

IEEE Photonics Society Japan Chapter

OECC/PS 2016: Program at a Glance

Day	Time	Room A 301-B	Room B 301-A	Room C 302-B	Room D 201-A	Room E 201-B	Room F 302-A
Sun. Jul 3	14:00-17:30	WS1	WS2	WS6	WS3	WS4	WS5
	17:30-18:00						
	18:00-20:00	Get together party					

Day	Time	Room A 301-B	Room B 301-A	Room C 302-B	Room D 201-A	Room E 201-B	Room F 302-A	Exhibition
Mon. Jul 4	09:00-09:15	Open Ceremony						10:00-16:30
	09:15-12:15	Plenary talks						
	12:15-14:30	Lunch & Exhibition						
	14:30-16:00	S1 Symposia:Optical access/core network evolution toward wireless 5G network era	MB1 High Spectral Efficiency Transmission	MC1 Multi-Core Fibers	MD1 High Speed VCSEL Links	ME1 Si Photonics Circuits	MF1 Photonic Signal Processing (I)	
	16:00-16:30	Coffee break						
	16:30-18:00	S1 Symposia:Optical access/core network evolution toward wireless 5G network era	MB2 Emerging Technologies	MC2 Spatial Mode Analysis	MD2 VCSEL	ME2 Switching Devices	MF2 Photonic Signal Processing (II)	

Day	Time	Room A 301-B	Room B 301-A	Room C 302-B	Room D 201-A	Room E 201-B	Room F 302-A	Exhibition
Tue. Jul 5	09:00-10:30	TuA1 Core Networks	TuB1 Advanced Modulation and Multiplexing	S4 Symposia:Commemorative symposium on IEEE Milestone for Vapor-phase Axial Deposition Method Optical Fiber: the beginning and perspectives toward future	TuD1 Advanced Lasers (I)	TuE1 Transmitters and Receivers	TuF1 Photonic Network System	10:00-16:30
	10:30-11:00	Coffee break						
	11:00-12:30	TuA2 Microwave Photonics for Mobile Access	TuB2 Digital Signal Processing	S4 Symposia:Commemorative symposium on IEEE Milestone for Vapor-phase Axial Deposition Method Optical Fiber: the beginning and perspectives toward future	TuD2 Electro-Optic Devices	TuE2 Mid IR and thermal applications	TuF2 Photonic Switching Network	
	12:30-14:00	Lunch						
	14:00-15:30	TuA3 New Direction of Optical Access Network	TuB3 Nonlinear Signal Processing	TuC3 Fiber Amplifiers	TuD3 Free Space and Short Distance	TuE3 Future Communication Components	S3 Symposia:Advanced Optical Technologies for Future Data Center Network	
	15:30-16:00	Coffee break						
	16:00-17:30	TuA4 Access Network Practicality	TuB4 Coding & Modulation Formats	TuC4 Active Fibers	TuD4 Multi Mode Fibers	TuE4 Devices for Silicon Photonics	S3 Symposia:Advanced Optical Technologies for Future Data Center Network	

Day	Time	Room A 301-B	Room B 301-A	Room C 302-B	Room D 201-A	Room E 201-B	Room F 302-A	Exhibition
Wed. Jul 6	09:00-10:30	WA1 Access Network Evolution	WB1 Coherent Optical Comminucation Technology	WC1 Optical Angular Momentum and SDM Related Technology	WD1 Active Devices on Si	WE1 Nonlinear Devices	WF1 Photonic Switching Technology (I)	10:00-14:30
	10:30-11:00	Coffee break						
	11:00-12:30	Poster Session						
	12:30-14:00	Lunch						
	14:00-15:30	WA3 Network Virtualization (I)	S2 Symposia:Space Division Multiplexing: Present Situation and Future Prospects	WC3 Fiber Sensors	WD3 Lasers for Communications	WE3 Dispersion Control	WF3 Photonic Switching Technology (II)	
	15:30-16 : 30	Coffee break						
	16:00-17:30	WA4 Network Virtualization (II)	S2 Symposia:Space Division Multiplexing: Present Situation and Future Prospects	WC4 Fiber Characterization	WD4 Modulators			
	18:30-20:30	Banquet						

Day	Time	Room A 301-B	Room B 301-A	Room C 302-B	Room D 201-A	Room E 201-B	Room F 302-A
Thu. Jul 7	09:00-10:30	ThA1 Recent Trends in Optical Networking	ThB1 Short Reach (I)	ThC1 SDM Related Fiber Devices & Connector	ThD1 Advanced Lasers (II)	ThE1 Photonic Tx/Rx	
	10:30-11:00	Coffee break					
	11:00-12:30	ThA2 Metro Networks	ThB2 Short Reach (II)	ThC2 SDM Amplifiers and Measurement	ThD2 Long Haul Transmission	ThE2 Photonics Switching System	
	12:30-13:30	Lunch					
	13:30-15:00	ThA3 Technical Challenge on Optical Access	ThB3 High-Speed Transmission	ThC3 Fiber Applications	ThD3 Receivers & Modulators	ThE3 Novel Materials and Devices	
	15:00-15:30	Coffee break					
	15:30-17:00	PDP					

WA2-66
Multi-Channel Lasing Characteristics for Linear-Cavity Fiber Sensor System using SOA and Fiber Bragg Grating Elements
Kazuto Takahashi(1), Mao Okada(1), Hiroki Kishikawa(1), Nobuo Goto(1), Yi-Lin Yu(2), Shien-Kuei Liaw(2)
(1)Tokushima Univ., Japan, (2)National Taiwan Univ. of Science and Technology, Taiwan
Multi-channel amplification with SOA is investigated for use in the proposed linear-cavity sensing system. The nonlinearity caused by gain saturation and FWM is analyzed. The lasing condition for multi-channel operation is also clarified.

WA2-67
Novel Soft-Cladding Optical Fiber for Distributed Pressure Sensing
Bin Zhou(1,2), Lin Htein(1), Zhengyong Liu(1), A. Ping Zhang(1), Chao Lu(1), Hwa-yaw Tam(1)
(1)The Hong Kong Polytechnic Univ., Hong Kong, (2) South China Normal Univ., China
A novel optical fiber with soft cladding is presented for surrounding pressure sensing application. The cladding is made of a kind of transparent silicone which can be compressed by and leads to extra loss. In the experiment the loss increment of a 0.5 meter long soft cladding fiber after applying high pressure up to 30 MP a is observed.

WA2-68
Novel Bidirectional Reflective Semiconductor Optical amplifier
G. de Valicourt(1), A. Maho(2), A. Le liepvre(2), R. Brenot(2), A. Velázquez(1,3), Y. K. Chen(1)
(1)Nokia, USA, (2)'Thales Research and Technology' and 'CEA Leti', France, (3)UNAM, Mexico
We propose a bidirectional reflective semiconductor optical amplifier as promising solution for on-chip amplification with silicon photonic integrated circuit. Small form factor device, wide optical bandwidth and high optical fiber-to-fiber gain are presented.

WA2-69
Semiconductor Optical Amplifier in AWG-STAR Network with Wavelength Path Relocation Function
Takumi Niihara(1), Minoru Yamaguchi(1), Osanori Koyama(1), Hiroaki Maruyama(1), Kazuya Ota(2), Makoto Yamada(1)
(1)Osaka Prefecture Univ., Japan, (2)Trimatiz Ltd., Japan
We constructed a semiconductor optical amplifier (SOA) unit with a signal gain greater than 20 dB, CWDM bandwidth amplification, low polarization dependence, and a low noise figure. To confirm the applicability of the SOA in an AWG-STAR network with our proposed wavelength path relocation function, we evaluated the power penalty of the SOA unit in an experimental AWG-STAR network. We found that amplification by the SOA unit was effective in making wavelength path relocation more flexible by compensating for accumulated optical losses due to optical devices used in the AWG-STAR network.

WA2-70
40Gb/s Optical Receiver Using High-Gain Multi-Level Active Feedback with Serial Inductor Peaking
Cheng-Ta Chan, Oscal T.-C. Chen
National Chung Cheng Univ., Taiwan
In this work, a high-gain wide-bandwidth optical receiver consisting of a trans-impedance amplifier, a limiting amplifier, and an output buffer is developed. Especially in each gain stage of a limiting amplifier, the high-gain 4'th-order Multi-Level Active Feedback (MLAF) structure with serial inductor peaking is employed to effectively increase the bandwidth and the gain. The TSMC 90nm CMOS technology was used to implement the proposed optical receiver. With the use of inductor peaking applied in the 4'th-order MLAF to enlarge the bandwidth, the proposed optical receiver has a bandwidth of 35GHz, and a differential trans-impedance gain of 86dBΩ. Comparing to conventional optical receiver, the proposed optical receiver exhibits a wide bandwidth, a high gain and fairly good performance for applications of 40Gbps optical communications.

WA2-71
Frequency Chirp Properties With Data Pattern Dependence in Quantum-Dot SOAs
Hiroki Hoshino, Norihiko Ninomiya, Motoharu Matsuura
The Univ. of Electro-Communications, Japan
We investigated the chirp properties using 10-Gbit/s signal with a fixed data pattern in quantum-dot semiconductor optical amplifiers. The results show that the properties depend on the data pattern affected by the gain recovery time.

WA2-72
Optical Sensor Based on Mach-Zehnder Interferometer Using Orbital Angular Momentum
Haozhe Yan, Shangyuan Li, Bian FengKai, Xiaoping Zheng, Hanyi Zhang, Bingkun Zhou
Tsinghua Univ., China
A novel Mach-Zehnder interferometric optical sensor using orbital angular momentum (OAM) is proposed and experimentally demonstrated by high order OAM beam with topological charge up to 10.

WA2-73
Precise Measurement of Microwave Evanescent Fields along Fiberglass-Reinforced Plastic Mortar Pipe Using Electro-Optic Sensor for Nondestructive Inspection
Yoshiyuki Azuma(1), Fumiaki Ueno(1), Hiroshi Murata(1), Yasuyuki Okamura(1), Tadahiro Okuda(2), Masaya Hazama(2)
(1)Osaka Univ., Japan, (2)Kurimoto LTD, Japan
We propose a new nondestructive inspection method for fiberglass-reinforced plastic mortar pipes using microwave guided-mode and photonic techniques. This method is based on precise measurement of microwave evanescent fields along the pipe-wall using electro-optic sensors.

WA2-74
Plasmon-induced Transparency based on Side-coupled Stub and Hexagonal Resonators and Its Sensing Characteristics
Tianye Huang(1,2), Minming Zhang(2), Songnian Fu(2)
(1)China Univ. of Geosciences, China, (2)School of optical and electronic information, and Huazhong Univ. of Science and Technolgy, China
A metal-insulator-metal (MIM) structure comprising stub and hexagonal resonator is proposed to realize plasmon-induced transparency (PIT) response. Benefit from high sensitivity and narrow transmission spectrum, sensing figure-of-merit as high as 178 RIU^{-1} can be achieved.

WA2-75
Optical Characteristicsof InP/GaInAs Core-multishell NWs Grown by Self-catalytic VLS Mode
Kohei Takano, Takehiro Ogino, Keita Asakura, Takao Waho, Kuzuhiko Shimomura
Sophia Univ., Japan
We have successfully demonstrated the growth of InP/GaInAs core-multishell nanowires employed the self-catalytic VLS mode and VPE mode of MOVPE, and obtained the photoluminescence spectrum dependent on the thickness of GaInAs shell layer.

WA2-76
S-K Growth of InAs Quantum Dots on Directly-bonded InP/Si Substrate Using MOVPE
Naoki Kamada, Toshiki Sukigara, Keiichi Matsumoto, Junya Kishikawa, Tetsuo Nishiyama, Yuya Onuki, Kazuhiko Shimomura
Sophia Univ., Japan
Stranski-Krastonogh QDs have been successfully grown on InP/Si substrate fabricated by wafer direct bonding. According to PL and AFM measurements, almost the same size and peak wavelength have been obtained with the InP substrate.

WA2-77
Hybrid Electro-optic Polymer Modulators
Feng Qiu, Shiyoshi Yokoyama
Kyushu Univ., Japan
In this letter, we report a TiO_2/electro-optic polymer hybrid rib-waveguide with a low figure of merit of 3.3 V·cm, corresponding to 1.65 V·cm in a traditional push-pull Mach-Zehnder interferometer structure. This low figure of merit results from the 80% improved poling efficiency of our EO polymer in the hybrid structure. The waveguide also possesses a relatively low propagation loss of 3.0 dB/cm and a simple fabrication process.

WA2-78
Photodetection Frequency Response Characterization for High-Speed Ge-PD on Si with an Equivalent Circuit
Jeong-Min Lee(1), Minkyu Kim(1), Stefan Lischke(2), Lars Zimmernman(2), Seong-Ho Cho(3), Woo-Young Choi(1)
(1)Yonsei Univ., Republic of Korea, (2)IHP, Germany, (3) Samsung Advanced Institute of Technology, Republic of Korea
We characterize photodetection frequency response of a waveguide-type Ge-PD on Si having larger than 50-GHz photodetection bandwidth using an equivalent circuit model. Our model provides accurate frequency responses and allows clear identification of different contributions.

WA2-79
Sub-μm Electrode Spacing SOI-PIN Photodiode Fabricated by CMOS Compatible Process
Hiroya Mitsuno, Takeo Maruyama, Koichi Iiyama
Kanazawa Univ., Japan
SOI-PIN photodiodes were fabricated by CMOS compatible processes. The -3dB bandwidth of 13 GHz was obtained at electrode spacing of 0.6 μm, receiving area of 20x20 μm^2 and pad area of 30x30 μm^2.

WA2-80
Comparison of Two Photodetector Linearity Characterizing Systems
Youxin Liu, Yongqing Huang, JiaRui Fei, Yangan Zhang, Xiaomin Ren, Kai Liu, Xiaofeng Duan
Beijing Univ. of Posts and Telecommunications, China
Two measurement techniques were investigated to characterize photodetector linearity. A model of the measurement system was developed to study the limitation of the two-tone method and the results correspond well to calculation results.

Photodetection Frequency Response Characterization for High-Speed Ge-PD on Si With an Equivalent Circuit

Jeong-Min Lee[1], Minkyu Kim[1], Stefan Lischke[2], Lars Zimmernman[2], Seong-Ho Cho[3], and Woo-Young Choi[1]
[1]Department of Electrical and Electronic Engineering, Yonsei University, Seoul, Korea
[2]IHP, Im Technologiepark 25, 15236 Frankfurt (Oder), Germany
[3]Mobile Health Care Group, Samsung Advanced Institute of Technology, Suwon-si, Gyeonggi-do, Korea
wchoi@yonsei.ac.kr

Abstract: *We characterize photodetection frequency response of a waveguide-type Ge-PD on Si having larger than 50-GHz photodetection bandwidth using an equivalent circuit model. Our model provides accurate frequency responses and allows clear identification of different contributions.*

Keywords: *Germanium photodetector, equivalent circuit model, Silicon photonics*

I. Introduction

Germanium photodetectors (Ge-PDs) realized on Si wafers are an essential component for Si photonic integrated circuits. Recently, Ge-PDs having photodetection bandwidth larger than 50-GHz have been reported [1] and high-performance monolithically integrated optical receiver circuits containing Ge-PDs have been demonstrated [2]. In order to achieve the optimal performance of integrated optical receivers, it is essential to have an accurate equivalent circuit model for Ge-PD that can be co-simulated with electronic circuits in the design stage. We have recently identified that the Ge-PD photodetection frequency response can be degraded with diffusion of photogenerated carriers and proposed an equivalent circuit model having two current sources, each of which respectively represents diffusion and drift of photogenerated carriers [3]. In this paper, we apply our modeling technique to the waveguide Ge-PD fabricated by IHP's photonic BiCMOS process, which has the unique capacity of integrating Si photonics devices with high-speed Si BiCMOS electronic circuits [4].

II. Equivalent Circuit Model

Fig. 1(a) shows the cross-section of the Ge-PD investigated in this paper. The intrinsic Ge layer is epitaxially grown on 220-nm thick, 750-nm wide Silicon-on-Insulator layer having 2-µm thick buried-oxide layer. The lateral PIN structure is realized with self-aligned implantation of P^+ and N^+ regions having peak concentrations of about 1×10^{18} cm^{-3} using 600-nm wide silicon nitride (SiN). The Ge-PD is 20-µm long. Details of the Ge-PD can be found in [1].

Fig. 1(b) shows the electron-hole pair generation rate due to absorption of 1.55-µm input light simulated with Lumerical 3-D FDTD, and Fig. 1(c) the electric-field distribution within our device biased at –1 V simulated with TCAD Sentaurus. As can be seen in the figures, a fair amount of electron-hole pairs are produced in the region where the electric field is not very strong and those carriers have to transport by slow diffusion. In order to accurately model the photodetection frequency response, consideration should be given to such this diffusion component as well as the drift process within the region having strong electric fields.

Fig. 2(a) shows the equivalent circuit model used in the present investigation. It has two current sources (I_1 and I_2) having different frequency responses for diffusion and drift of photogenerated carriers. Each current source has the single-pole frequency response with time constant τ_1 for I_1 and τ_2 for I_2, along with corresponding DC gain, A_1 and A_2,

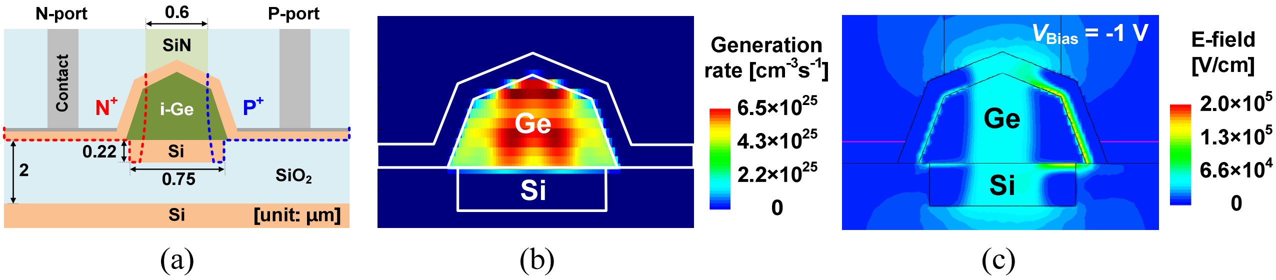

Fig. 1. (a) Cross-section of Ge-PD, (b) 3D-FDTD simulated generation-rate profile, and (c) simulated electric-field distribution at –1 V.

sum of which represents Ge-PD DC responsivity, normalized to one for simplicity in this paper. Z_{para} in the model represents passive electrical components due to interconnect, pad, parasitic resistances and capacitances. Specifically, R_{int} and L_{int} represent interconnect resistance and inductance, respectively, C_{pad} pad capacitance, C_{ox} oxide capacitance, R_{si} bottom silicon substrate resistance, and $C_{c\text{-}c}$ capacitance between contacts. For modeling PIN junction, R_s represents series resistance, C_j depletion capacitance, and R_j depletion resistance.

S-parameters are measured for open and short test patterns on the same wafer with a vector network analyzer from 100 MHZ to 67 GHz, from which numerical values for R_{int}, L_{int}, C_{pad}, C_{ox}, and R_{si} are determined as 1.4 Ω, 56 pH, 16.7 fF, 30 fF, and 2 kΩ, respectively. Measured *S*-parameters of Ge-PD are used for extraction of R_s, C_j, R_j, and $C_{c\text{-}c}$ values. The extracted values are listed in Table I.

To extract current source model parameters, the generation rate profile shown in Fig. 1(b) is imported into TCAD Sentaurus and two virtual generation rate profiles are created as shown in Fig. 3(a) and (b), one containing the generation rate only in the region where electric field is weak (< 2000 V/cm), representing the region where photogenerated carriers experience diffusion as shown in Fig. 3(a), and the other in the region where the electric field is strong (> 2000 V/cm), representing the region where photogenerated carriers experience drift in Fig. 3(b), respectively. Then we perform photodetection frequency response simulation for each case using TCAD Sentaurus and the results are fitted with single-pole frequency responses as can be seen Fig. 3(c). From these, we extract current source model parameters of τ_1 and A_1 for I_1, and τ_2 and A_2 for I_2 as listed in Table II. At –1-V bias voltage, about 9.2% of photogenerated carriers experience diffusion with the corresponding time constant of 15.9 ps.

III. Photodetection Frequency Response Characterization

Fig. 4(a) shows the measured photodetection frequency response and the simulated result with our equivalent circuit. As can be seen, they agree well confirming the accuracy of our model. Using our equivalent circuit model, we can identify the contribution of each factor that influences the photodetection frequency responses. Fig. 4(b) shows the simulated results considering only τ_{RC} (without current sources in the equivalent circuit), τ_1 and τ_2 (without *RC* components), and τ_2 (without current source for diffusion and *RC* components). For these simulations, only the Ge-PD core is considered without Z_{para}. As can be seen in the figure, the photodetection bandwidth is limited by carrier transport and the diffusion of photogenerated carriers further degrades the photodetection bandwidth. It should be also noted that the bandwidth limitation due to parasitics is not very significant due to the optimized fabrication process providing very small parasitic resistances. This type of identification can be of great help for further device optimization.

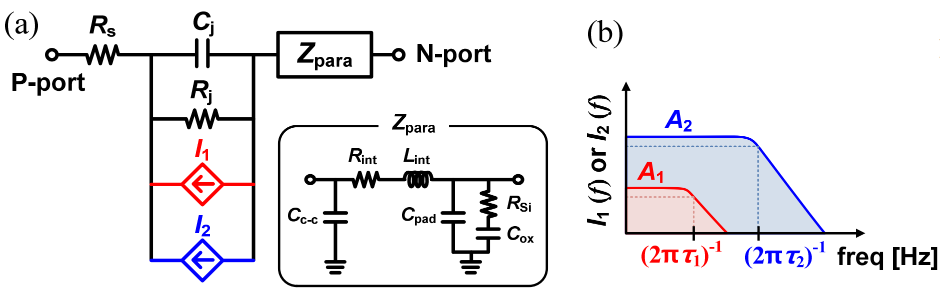

TABLE I
Extracted RC Parameters of Ge-PD at -1V

R_s [Ω]	80
C_j [fF]	7.2
R_j [kΩ]	100
$C_{c\text{-}c}$ [fF]	3.2
τ_{RC} [ps]	0.9

Fig. 2. (a) A modified equivalent circuit model of Ge-PD and (b) frequency responses of photogenerated current source models.

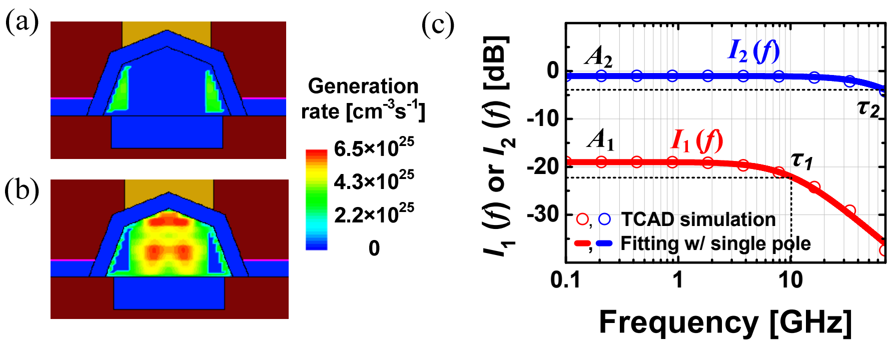

TABLE II
Extracted Current Source Model Parameters at -1V

τ_1 [ps]	15.9
A_1 [%]	9.2
τ_2 [ps]	2.3
A_2 [%]	90.8

Fig. 3. Virtual generation-rate profiles of photogenerated carrier (a) diffusion and (b) drift, and (c) simulated photodetection frequency responses of two current source models at –1 V.

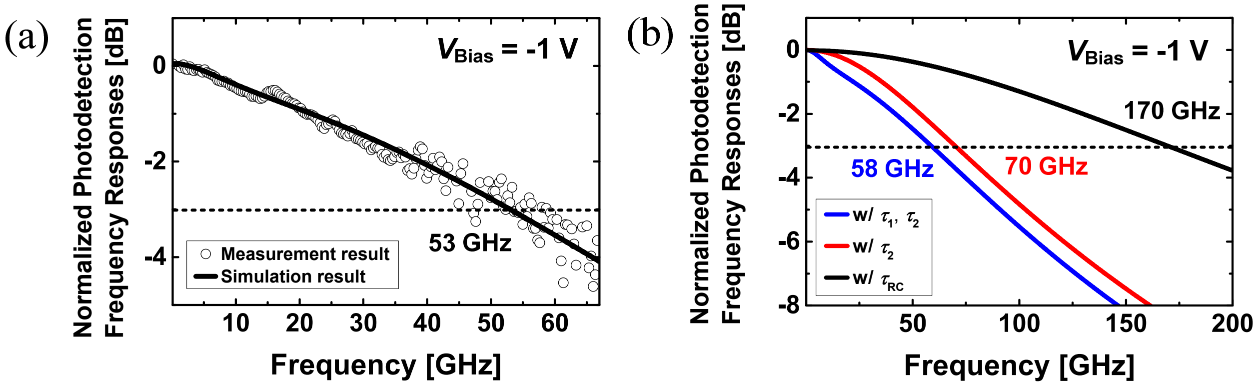

Fig. 4. (a) Measured and simulated photodetection frequency response and (b) simulated frequency responses with different time constant contributions.

IV. Conclusions

We present an equivalent circuit model for waveguide-type Ge-PD on Si having greater than 50-GHz photodetection bandwidth and show how to extract model parameters for Ge-PD. Using our equivalent circuit model, we can identify those factors that limit the photodetection frequency response. Our equivalent circuit can be of great help in designing high-performance monolithic integrated optical receivers.

Acknowledgment

Manuscript received. This work was supported by the National Research Foundation of Korea grant funded by the Korea government [2015R1A2A2A01007772].

References

[1] S. Lischke et al., "High bandwidth, high responsivity waveguide-coupled germanium p-i-n photodiode," Opt. Exp., vol. 23, no. 21. pp. 27213-27220, Oct. 2015.
[2] A. Awny et al., "A 40 Gb/s monolithically integrated linear photonic receiver in a 0.25 µm BiCMOS SiGe:C technology," IEEE Microw. Compon. Lett., vol. 25, no.7, pp. 469-471, July 2015.
[3] J.-M. Lee and W.-Y. Choi, "An equivalent circuit model for germanium waveguide vertical photodetectors on Si," in Proc. MWP/APMP, 2014, pp. 139-141.
[4] L. Zimmermann et al., "BiCMOS silicon photonics platform," in Proc. Opt. Fiber Commun. Conf. (OFC), 2015, pp. 1-3.